On electrostatic interactions of ATP-IDE revealed by quantum mechanics/molecular mechanics (QM/MM) and molecular dynamics (MD)

Sarawoot Somin[1,2], Don Kulasiri[1,2,*] and Sandhya Samarasinghe [1]
[1]Centre for Advanced Computational Solutions (C-fACS), Lincoln University, Christchurch 7647, New Zealand.

[2]Department of Molecular Biosciences, Lincoln University, Christchurch 7647, New Zealand

[*]Correspondence: don.kulasiri@lincoln.ac.nz

Abstract

Background: The insulin-degrading enzyme (IDE) plays a significant role in the degradation of the amyloid beta (Aβ), a peptide found in the brain regions of the patients with early Alzheimer's disease (AD). Adenosine triphosphate (ATP) allosterically regulates the Aβ-degrading activity of IDE. The present study investigates the electrostatic interactions between ATP-IDE at the allosteric site of IDE, including thermostabilities/flexibilities of IDE residues, which have not yet been explored systematically.

Methods: This study applies the QM/MM to the proposed computational model for exploring electrostatic interactions between ATP and IDE. MD simulations are performed at different temperatures for identifying flexible and thermostable residues of IDE.

Results: The proposed computational model predicts QM/MM energy-minimised structures providing the IDE residues (LYS530 and ASP385) with high binding affinities. Considering root mean square fluctuation (RMSF) values during the MD simulations at heat-shock temperatures, it indicates that LYS530 and ASP385 are also the thermostable residues of IDE, whereas SER576 and LYS858 have high flexibilities with compromised thermostabilities.

Conclusions: The present study sheds light on the phenomenon of biological recognition and interactions at the ATP-binding domain which may have important implications for pharmacological drug design. The proposed computational model may facilitate the development of allosteric IDE activators/inhibitors which mimic ATP interactions.

Keywords: electrostatic interactions; QM/MM Calculation method; molecular dynamic simulation, thermostability/flexibility

Author summary: *ATP acts as an allosteric regulator of IDE in Aβ clearance (the degradation of Aβ). Computational methods for the electrostatic interactions of ATP-IDE interactions and molecular dynamics (MDs) of IDE are essential for the pharmacological drug design against early AD. The proposed model involving QM/MM calculation and MD simulations, is developed to explore the electrostatic interactions of ATP-IDE interactions and MDs of IDE at different temperatures. Subsequently, the electrostatic interactions between atoms of ATP-IDE interactions and the thermostabilities/flexibilities of IDE residues are elucidated.*

1 INTRODUCTION

The Aβ peptides play a significant role in the development of AD by aggregating abnormally, forming senile plaques that block neurotransmitters in the synapses. Furthermore, the Aβ peptides induce the activation of intracellular kinases, leading to the phosphorylation of tau proteins. These proteins play a crucial role in stabilising microtubules, abundant in neurons. In this phosphorylated state, the tau proteins detach themselves from microtubules, triggering an inflammatory response and the development of neurofibrillary tangles. However, the Aβ peptides are produced naturally in the brain as a byproduct of the normal metabolism of amyloid precursor protein (APP) [1]. In healthy conditions, the Aβ peptides are removed from the brain by several processes of Aβ clearance, in particular Aβ degradation. In preclinical phase of AD, dysfunctional Aβ clearance, caused by imbalance between Aβ degradation and Aβ aggregation – the Aβ aggregation outweighs

the Aβ degradation, contributes to extracellular senile plaque deposits and intracellular neurofibrillary tangles [2].

The Aβ peptides play a central role in Aβ aggregation and thus, are of interest for the treatment of early AD [3, [4]. The insulin-degrading enzyme (IDE), a Zn^{2+} metalloprotease from the M16 family, helps degrade the Aβ peptides and facilitate Aβ clearance [5]. The Aβ-degrading activity of IDE includes four stages. Firstly, IDE exists in an active form. Subsequently, in its active state, the Aβ peptide migrates into the catalytic chamber, prompting IDE to close and initiate the degradation process. The final step involves IDE returning to an open conformation, facilitating the release of the degraded product. IDE is composed of 970 residues and is comprised of two halves: the N-terminal and the C-terminal [6, [7]. The catalytic chamber is made up of two halves, formed by a flexible loop or a crypt. This crypt has electrostatic properties (a negative interior - IDE-N and a positive interior - IDE-C), which enables it to open and close. The IDE-N contains domains 1 and 2, and IDE-C halves contain domains 3 and 4. When 'closed', the dimensions of domains 1 to 4 are approximately 16,000 $Å^3$ in volume (excluding the flexible loop of 80 amino acids) [8, [9, [10]. The active site is in domain 1 of the IDE-N which contains a water molecule and the Zn^{2+} binding motif coordinated by three crucial amino acids: HIS108, HIS112, and GLU189 [11]. The allosteric site, the non-catalytic site, is located in domain 2 away from the active site (30 Å), which facilitates interactions at the substrate – in particular the Aβ peptides – and activates related subunits via allosteric effect (Figure 1) [12, [13].

The ATP has been identified as an allosteric inhibitor which causes a reduction in large-Aβ-peptide (such as Aβ42 peptide) degradation, leading to accumulation of Aβ in the brain [14, [15, [16]. However, an in vivo study has identified that the presence of ATP, including Mg^{2+}, helps to degrade the short Aβ peptides [17]. Many studies have also reported that ATP may enhance IDE activity related to short peptides such as insulin and glucagon [9, [15, [16]. ATP enhances the short-peptide degradation by modifying the structure of IDE. It shifts the quaternary structure of IDE from dimers to monomers and breaks electrostatic equilibrium responsible for maintaining the closed form of IDE. This process results in an increased population of open form of IDE and enhanced catalytic turn over during the short-peptide degradation [9, [15, [18]. Kinetic studies have found that a reduction in the enzyme affinity of the IDE and the Aβ peptides, caused by the synthesis of ATP, results in a reduction of Aβ degradation [15, [16]. These studies imply that while ATP inhibits IDE from degrading the long Aβ peptides, it enhances IDE's ability to degrade short Aβ peptides. However, the interactions between ATP and the ATP-binding domain within IDE, particularly at the electronic level, remain unclear.

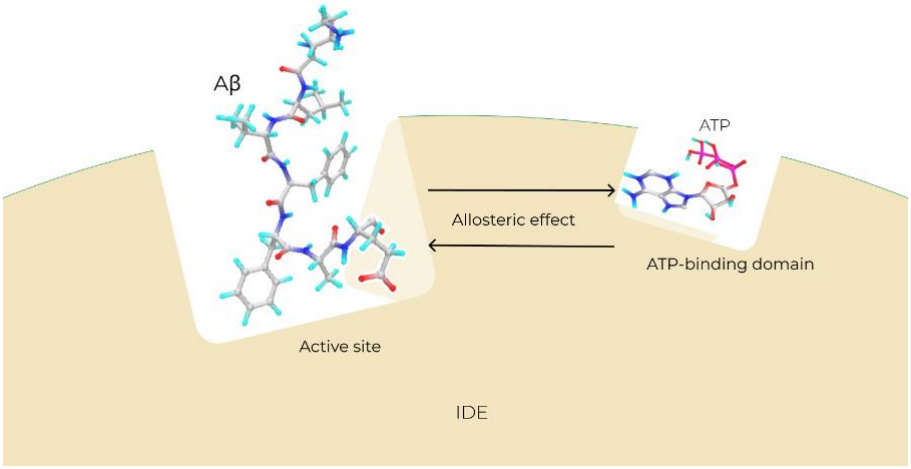

Figure 1. Allosteric effects. The interaction of ATP with IDE at the ATP-binding domain regulates the Aβ degradation via the allosteric effect. Also, the interaction of Aβ peptide at the active site may influence a conformational change at ATP-binding domain via the allosteric effect.

A substrate itself may serve as an allosteric activator, known as cooperativity (Figure 1) [19]. This cooperativity can induce structural conformational changes in the protein through long-range effects. For example, the interactions of haem groups, far apart (40 Å) from the direct interaction, have been identified as the cooperative binding causing the conformational changes in haemoglobin through the long-range effects [20, [21]. Likewise, the Aβ peptides have also been identified as the allosteric modulators of cholinesterases, a group serine hydrolase which regulates nerve transmission [22]. This study showed that the interactions of Aβ peptides with the cholinesterases at the active site cause the conformational changes of molecules in the system, leading to an increase in an influx of acetylcholine into the catalytic site –regulating the nerve transmission. As the X-ray crystal structure have shown that the allosteric site of IDE is in a region 30 Å away from the active site [13], there is a high propensity that presence of an Aβ peptide at the active site may cause the conformational changes at the ATP-binding domain.

Biological interactions, comprised of intermolecular interactions, proximity and topological properties of electron density, provide information to indicate the binding affinity of ATP towards IDE residues at the ATP-binding domain. These biological interactions are also critical in development of active substances, the central topic of pharmacological drug design [23, [24]. The forces underlying these interactions include electrostatic interactions, van der Waals forces, salt bridge. Understanding the biological interactions relies on essential information about electrostatic interactions, including ionic bonds, as well as polar and nonpolar covalent bonds [25, [26, [27]. Also, a hydrogen bond is regarded as an electrostatic interaction between a hydrogen-atom, covalently bonded to an electronegative donor atom (D), and electronegative acceptor atom (A). The electrostatic interactions has been analysed for the selection of a target and evaluation of lead compounds for drug design [25]. Strong-weak hydrogen bonds in the environment of allosteric regulation have been discriminated for optimisation of the lead compounds [28]. There two types of hydrogen bonding: classical hydrogen bond and non-classical hydrogen bond. The classical hydrogen bond involves a hydrogen atom located between a pair of a strong-electronegative atoms, with one acting as D, and another strong-electronegative atom, acting as A. This interaction is represented by D-H···A. For example, a hydrogen bond between oxygen involves a strong donor and a strong acceptor: O-H···O. A non-classical hydrogen bond occurs when a weak donor, such as carbon, indirectly attaches to the strong receptor, interacting with the donor through electrostatic interactions (π); for example, C-H···π. While a classical hydrogen bond is a strong bond, a non-classical hydrogen bond is a weak bond.

Charge-density analysis, which involves evaluating the distribution of charge-density and electrostatic interactions, is used to characterise intermolecular interactions and to obtain information about the topological properties of electron density. X-ray diffraction has been employed to furnish data for analyses of charge-density [29, [30, [31]. Ligand-protein complex studies have applied X-ray diffraction to the charge-density analysis method to understand ligand-protein complexes at different subatomic resolutions of X-ray diffractometers such as 0.69 Å resolution, 0.65 Å resolution, and 0.48 Å resolution [29, [30, [31]. However, these subatomic resolutions are still limited in their ability to image single atoms of interest due to the low quality of the crystals, caused by crystal defects during X-ray diffraction processes – or a catalysation of processes. This limitation can be overcome using the QM/MM calculation, enabling the computation of individual atoms of interest [27, [32, [33]. For instance, the QM/MM calculation has been used to minimise the systems, called QM/MM minimisation, for exploring the chemical bonding nature of oestrogen molecules (estrone, 17b-estradiol and estriol hormones) in the oestrogen-binding domain [27]. This study has identified non-covalent bonds of oestrogen molecules and the receptors with high affinity, considering the intermolecular interactions, and the topological properties of electron density.

Thermostabilities and flexibilities of the residues of interest are also essential for the thermostable and flexible optimisation of drug design [34, [35]. Thermostability has been discussed to design the lead compounds with higher activity and specificity [35]. Likewise, researchers have identified that the residues with flexibilities play a crucial role for reducing proteolytic susceptibility of protein drug [36]. In MD studies, the RMSF values have been applied to identification of residues with flexibilities such as an isomerase and extremophilic bacterium [35, [37, [38]. For instance, the RMSF values during the MD simulation at the heat stress have been elucidated for understanding thermostability and folding/unfolding of residues of SazCa (a thermophilic bacteria) [35]. The

MD simulations with RMSF have been used to select mutants that improve the catalytic performance of the γ-lactamase (an enzyme produced by bacteria development of novel biocatalysts) [39]. Therefore, gaining insights into the thermostabilities and flexibilities of IDE residues within ATP-binding domains through MD simulations may assist researchers in pharmacology to explore specific residues for drug design, aiming for enhanced activity and specificity. Generally, researchers conduct the MD simulation to explore flexibilities/thermostabilities at different and specific temperatures. For example, researchers also consider specific temperatures to explore the thermostabilities of residues. Recently, researchers have conducted the MD simulation to explore flexibilities/thermostabilities of single-domain antibodies under different specific temperatures (300 K, 400 K, 500 K) [40]. A study used the MD simulations at 310 K to elucidate the enzymatic reaction of Phenazine Biosynthetic Protein, showing the regions with high flexibilities [38]. To explore the reaction of Aβ degradation by IDE, the MD simulations have been conducted at 300 K [18, [41]. An in vitro experiment has investigated a response of IDE as the heat-shock response, the response by protein folding and re-folding or activating autophagy induced by heat stress, in different human cell lines (SHSY5Y, NHLF and PBL cells). Researchers have revealed that the heat-shock responses of IDE are expressed at 321.15 K in SHSY5Y and NHLF cells, whereas 315.15 K in PBL cell [42]. Practically, the heat-shock response of biological organisms of interest has been measured to provide insight into an assay for drug screening [43].

As we mentioned above, QM/MM simulation studies have reported the biomolecular interactions between IDE and Aβ peptide. The systematic understanding of electrostatic interactions in ATP-IDE interactions, which may be influenced by the presence of the Aβ peptide, has not been fully comprehended. Furthermore, the thermostabilities/flexibilities of the IDE residues at the ATP-binding domain have never been elucidated during the MD simulations at the heat-shock temperatures. Therefore, the present study employs the QM/MM calculation method to minimise the systems for exploring ATP atoms forming the electrostatic interactions with IDE atoms. Then, we discuss the intermolecular interactions, the proximity and the topological properties of electron density for investigating the binding affinity of ATP towards the IDE residues at the ATP-binding domain. The present study also uses the RMSF to measure flexibilities/thermostabilities of IDE residues at the interacting surface of the ATP-binding domain during the MD simulation at the 300K and the heat-shock temperatures (315.15 K and 321.15 K).

2 RESULTS AND DISCUSSION

Both the ATP-IDE and the ATP-IDE-Aβ systems were constructed to differentiate and explore the dependent action of the IDE residues as receptors of the biological ATP interaction. We performed molecular docking for molecular docking analysis. The lowest docked energy conformers of ATP in both ATP-IDE and ATP-IDE-Aβ systems were selected to prepare the initial structures of the simulations. After QM/MM minimisation, we explored ATP forming electrostatic interactions with IDE, considering the intermolecular interactions, the proximity and the topological properties of electron density. This study did not analyse non-classical hydrogen bonds, as they form between weak donors and weak acceptors. The results of this study revealed the electrostatic interactions with high affinities, including thermostable/flexible residues of IDE.

2.1 Molecular docking

We conducted 10 conformers of ATP, with the corresponding free energies (kcal mol^{-1}), based on classical force field energy calculations, available in the Supplementary Table S4 and Fig. S1. Each conformer was optimised, using docking free energy calculations [44], until it reached the maximum number of interactions possible or stable free energy.

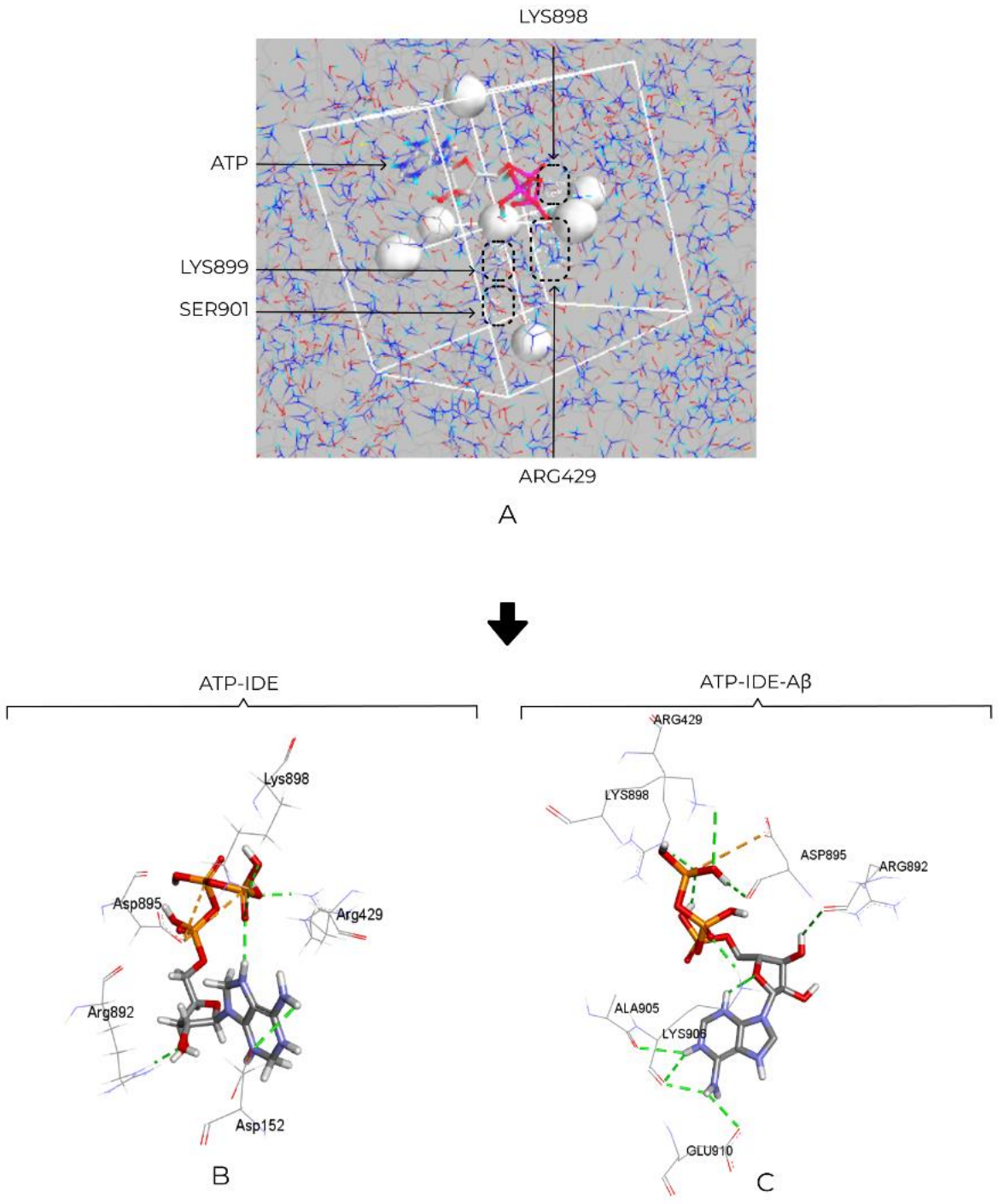

Figure 2. Molecular docking and conformers after the simulations. (A) The search region covering the ATP-binding positions (ARG429, LYS898, LYS899, SER901). (B) The conformer after the simulation in the ATP-IDE system, with the electrostatic interactions between ATP and IDE residues (the hydrogen bonds: ASP152, ARG429, ARG892, ASP895, LSY898; the polar covalent bond: ASP895). (C) The conformer after the simulation in the ATP-IDE-Aβ system, with the interactions between ATP and IDE residues (the hydrogen bonds: ARG492, ARG892, ASP895, LYS898, ALA905, LYS906, GLU910; the polar covalent bond: ASP895). The dotted green line and the dotted orange line represent the hydrogen bonds and the polar covalent bonds, respectively.

2.2 QM/MM interactions

After conducting QM/MM minimisation using the Ambertools package (https://ambermd.org/AmberTools.php), the conformers of ATP-IDE interactions were generated. This process resulted in the seqeunce number of residues different from 2wk3 crystal structure from the Protein Data Bank (Table 1). We illustrated the interactions between ATP and IDE using BIOVIA discover studio visualiser software (https://www.3ds.com/products-services/biovia/). The simulation output revealed electrostatic interactions of ATP-IDE, including hydrogen bonds, polar covalent bonds and nonpolar covalent bonds (Figure 3).

Table 1. Residues names in 2wk3 crystal structure from the Protein Data Bank, and residue names in QM/MM minimised structures.

Residue name (2wk3)	Residue name after QM/MM minimisation
LYS425	LYS384
ASP426	ASP385
GLU428	GLU387
LYS571	LYS530
LYS573	LYS532
SER617	SER576
SER634	SER593
LYS899	LYS858
LYS901	LYS860

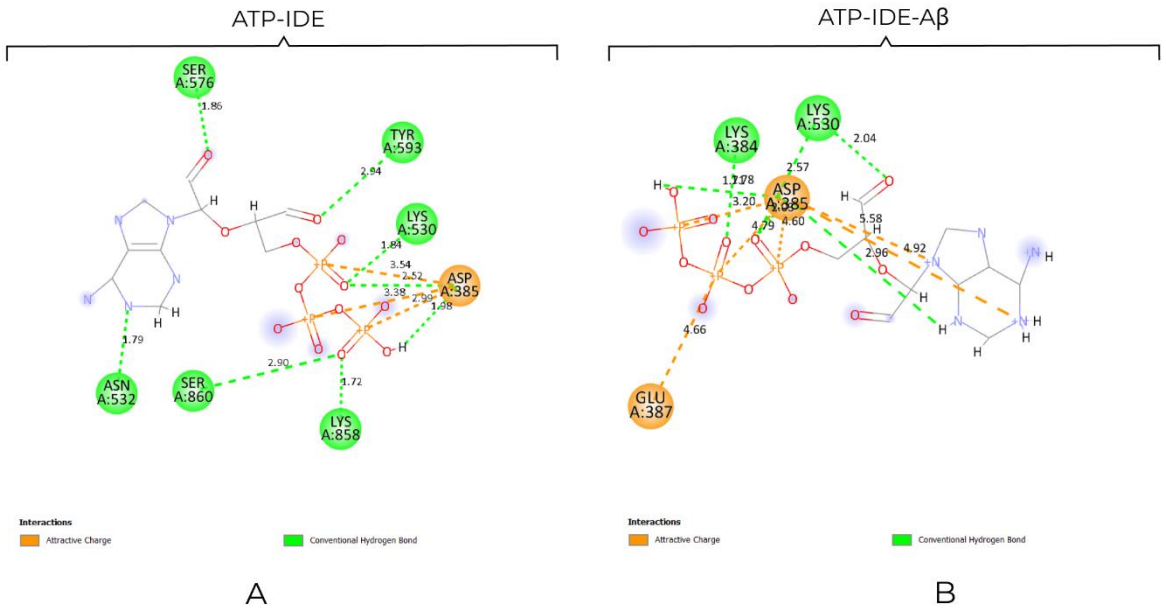

Figure 3. The hydrogen bonds and attractive charges (polar/nonpolar covalent bonds) of ATP-IDE in the ATP-IDE system (A) and ATP-IDE-Aβ system (B), after QM/MM minimisation. The line structure represents ATP, which interact with the IDE resides through hydrogen bonds (green ball) and polar/nonpolar covalent bonds (orange ball). The dotted green line and the dotted orange line represent the classical hydrogen bonds and the attractive charges, respectively.

Table 2. The intermolecular interaction of electrostatic interactions between the ATP and the APT-binding domain within the IDE allosteric site, after QM/MM minimisation.

ATP	IDE	Type	Distance (Å)	
			ATP-IDE system	ATP-IDE-Aβ system
N2	ASN532 (HD22)	Hydrogen bond	1.79	
O1	SER576 (HG)	Hydrogen bond	1.86	
O12	TYR593 (HN)	Hydrogen bond	2.94	
O7	LYS858 (HZ3)	Hydrogen bond	1.72	
O7	SER860 (HG)	Hydrogen bond	2.9	
O3	LYS530 (HZ3)	Hydrogen bond	1.84	2.57
O3	ASP385 (HN)	Hydrogen bond	2.52	2.03
H5	ASP385 (OD2)	Hydrogen bond	1.98	1.71
P	ASP385 (OD2)	Polar covalent bond	3.54	4.6
P1	ASP385 (OD2)	Polar covalent bond	3.32	4.79
P2	ASP385 (OD2)	Polar covalent bond	2.99	3.2
O12	LYS530 (HZ1)	Hydrogen bond		2.04
O5	LYS384(HZ1)	Hydrogen bond		1.78
HN	ASP385 (OD2)	Hydrogen bond		2.96
N	ASP385 (OD2)	Nonpolar covalent bond		5.58
N2	ASP385 (OD2)	Nonpolar covalent bond		4.92
P1	GLU387 (OE2)	Polar covalent bond		4.66

2.3 Intermolecular interactions

According to the data in Table 2, there are nine IDE residues (LYS384, ASP385, GLU387, LYS530, ASN532, SER576, TYR593, LYS858, SER860) involved in the electrostatic interactions (hydrogend bond, polar covalent bond and nonpolar covalent bond) in both systems. To identify the binding affinity of ATP towards an allosteric site of IDE, we elucidated the intermolecular interactions between the ATP and the IDE residues at the ATP-binding domain. The ATP-IDE system contained eight hydrogen bonds and three polar convalent bonds, while ATP form four polar covalent bonds, two nonpolar covalent bond and six hydrogen bonds with IDE in the ATP-IDE-Aβ. In the ATP-IDE system, there are six oxygen-atoms and a nitrogen-atom of ATP as the accepters, and another one hydrogen-atom of ATP as the donor. These atoms formed eight hydrogen bonds with IDE. In the ATP-IDE-Aβ system, there were a hydrogen-atom (as the donor) and four oxygen-atoms (as the acceptors) of ATP forming the hydrogen bonding interaction with oxygen and hydrogen-atoms of IDE. For the remaining interaction, a phosphorus-atom and two nitrogen-atoms of ATP formed polar/nonpolar interactions with oxygen-atoms of IDE.

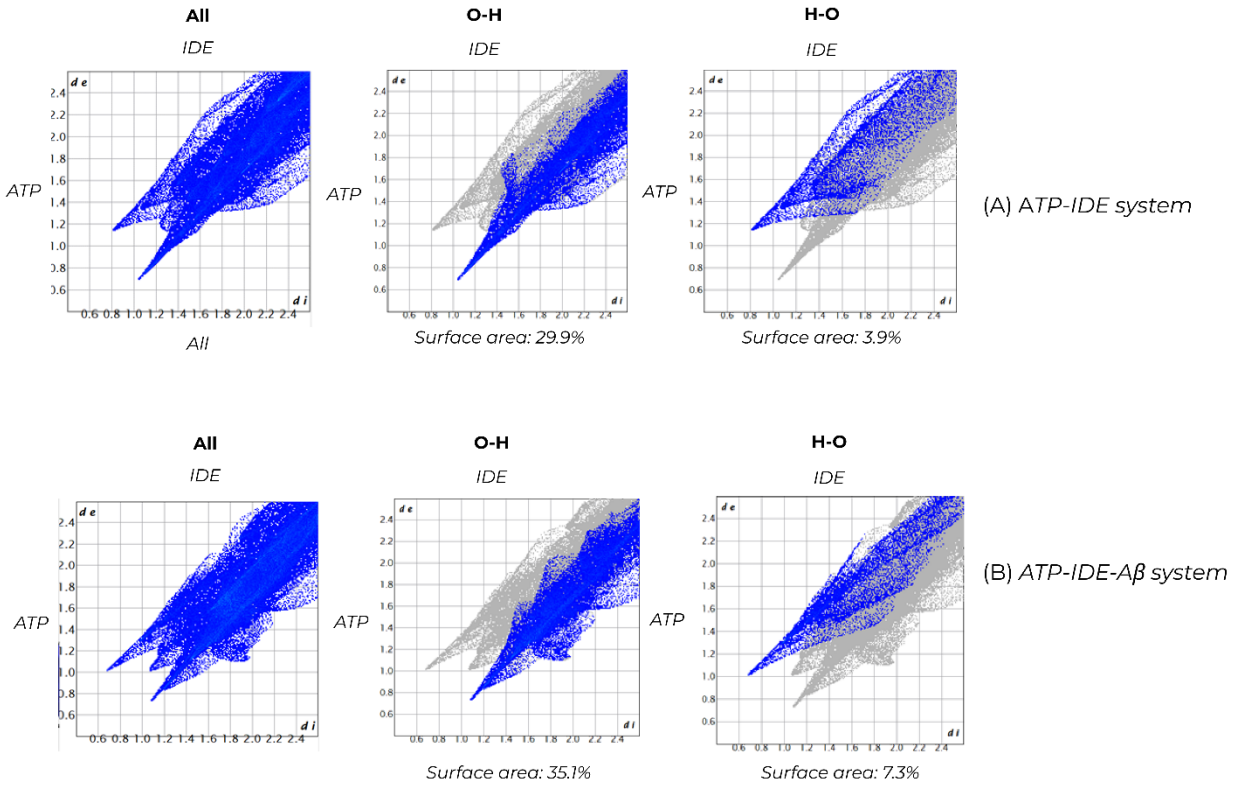

Figure 4. Surface area of hydrogen bonding interactions between ATP atoms and IDE residues through Hirshfeld surface. The hydrogen bonding interactions of Hirshfeld surface with ATP and IDE nuclei represented in dot blue. The distance between the Hirshfeld surface and nearest nucleus of ATP is represented by *di*, whereas *de* represents the Hirshfeld surface and nearest nucleus of IDE. (A) Hirshfeld surface analysis of the hydrogen bonding interaction of ATP-IDE system. (B) Hirshfeld surface analysis of the hydrogen bonding interaction of ATP-IDE-Aβ system.

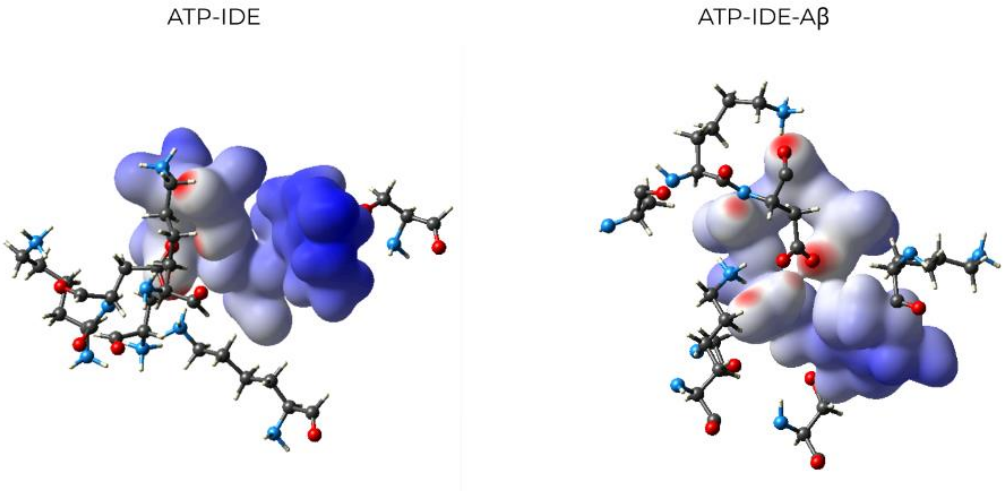

Figure 5. The Dnorm maps of ATP-IDE and ATP-IDE-Aβ systems. These Dnorm maps, based on the density functional theory (DFT) calculation, shows the electron density of ATP after QM/MM minimisation, with the ATP's proximity to the IDE residues. Both systems are shown using the same angle and settings. The red, white, and blue indicate close, medium, and little proximity, respectively.

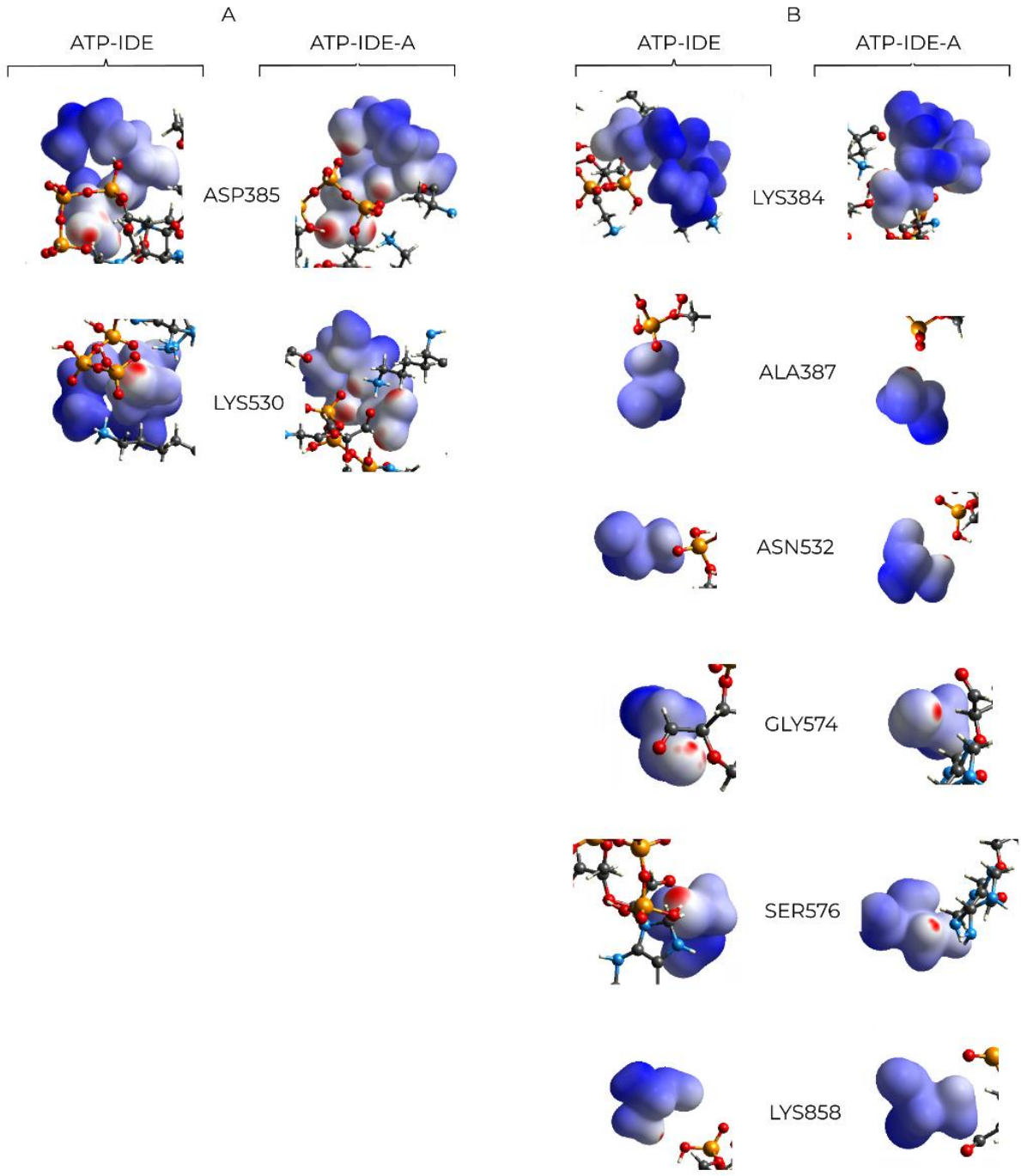

Figure 6. The Dnorm map, based on the DFT calculations, shows the electron density of the IDE residues at the ATP-binding domain in both ATP-IDE and ATP-IDE-Aβ. (A) the residues with close proximity including ASP385 and LYS530. (B) The residues with medium and little proximity including LYS384, ALA387, ASN532, GLY574, SER576 and LYS858.

2.4 Analysis of the topological properties of electron density

The topological distance and energies of the interactions were calculated using the MoPro package to furnish a description of the topological properties [45]. Critical points are specific locations within the electron density

distribution of a molecule where the gradient of the electron density is zero, found between the nuclei where the first derivative of electron density vanishes ($\nabla\rho(r) = 0$) [46, [47]. These critical points contribute a quantum description of molecule bonds. Topological distance refers to the distance from the critical point to the nuclei of the ATP and the IDE residues (D_{cp1}, D_{cp2}). The Laplacian of electron density ($\nabla^2\rho(r)$) was used to measure the kinetic and potential energy densities at the critical point [48]. $\nabla^2\rho(r) < 0$ means that the bonding region is dominated by lowering potential energy, $\nabla^2\rho(r) > 0$ means that the bonding region is dominated by excess kinetic energy which creates a repulsive force [49]. We also calculated the kinetic and potential energy density (T, V) and the sum of T and V (H(r)) using MoPro Package, where $|V|/T > 1$ and $H(r) < 0$ correspond to a strong interaction with partial covalent bonding interaction, and $|V|/T < 1$ and $H(r) > 0$ correspond to a weak interaction with closed shell type of interaction [50].

We calculated topological properties and the energies of the QM/MM minimised structure from both the ATP-IDE and the ATP-IDE-Aβ systems for topological analysis (Table 3). The polar covalent bonds in both the ATP-IDE and the ATP-IDE-Aβ systems created high $\rho_{bcp}(r)$ due to the strong force of the polar covalent bonds.

Table 3. The topological distance and energies of the interactions. T: kinetic energy density (kJ/mol/Bohr^3); V: potential energy density (kJ/mol/Bohr^3); H(r): the sum of kinetic energy and potential energy; $\rho_{bcp}(r)$: electron density (eÅ^{-3}); $\nabla^2\rho(r)$: Laplacian of electron density (eÅ^{-5}).

ATP atoms	IDE residues	V	T	|V|/T	H(r)	$\rho_{bcp}(r)$	$\nabla^2\rho(r)$
ATP-IDE							
N2	ASN532 (HD22)	-0.0376	0.024	1.567	-0.0136	0.15812	1.531
O1	SER576 (HG)	-0.029	0.03	0.967	0.001	0.15812	1.633
O12	TYR593 (HN)	-0.018	0.022	0.818	0.004	0.09814	1.214
O7	LYS858 (HZ3)	-0.0331	0.023	1.439	-0.0101	0.16014	1.712
O7	SER860 (HG)	-0.049	0.053	0.925	0.004	0.10014	1.359
O3	LYS530 (HZ3)	-0.207	0.206	1.005	-0.001	0.29527	2.578
O3	ASP385 (HN)	-0.067	0.022	3.045	-0.045	0.09964	1.314
H5	ASP385 (OD2)	-0.21	0.209	1.005	-0.001	0.10665	2.024
P	ASP385 (OD2)	-1.917	1.648	1.163	-0.269	1.04586	7.507
P1	ASP385 (OD2)	-0.908	0.153	5.935	-0.755	1.54591	8.887
P2	ASP385 (OD2)	-1.008	0.024	42.000	-0.984	1.74599	9.001
ATP-IDE-Aβ							
O3	LYS530 (HZ3)	-0.067	0.025	2.680	-0.042	0.08764	1.245
O3	ASP385 (HN)	-0.067	0.028	2.393	-0.039	0.10964	1.398
H5	ASP385 (OD2)	-0.301	0.209	1.440	-0.092	0.30665	2.612
P	ASP385 (OD2)	-1.907	1.658	1.150	-0.249	1.05986	7.521
P1	ASP385 (OD2)	-1.892	1.673	1.131	-0.219	1.04416	7.506
P2	ASP385 (OD2)	-1.877	1.673	1.122	-0.204	1.13986	8.501
O12	LYS530 (HZ1)	-0.128	0.227	0.564	0.099	0.11064	1.399
O5	LYS384(HZ1)	-0.754	0.425	1.774	-0.329	0.11438	2.127
HN	ASP385 (OD2)	-0.129	0.854	0.151	0.725	0.10014	1.282
N	ASP385 (OD2)	-2.012	3.978	0.506	1.966	0.47286	2.531
N2	ASP385 (OD2)	-3.087	2.978	1.037	-0.109	0.67226	2.834
P1	GLU387 (OE2)	-1.887	1.678	1.125	-0.209	1.07286	7.021

2.5 Analysis of the thermostabilities and flexibilities of IDE residues

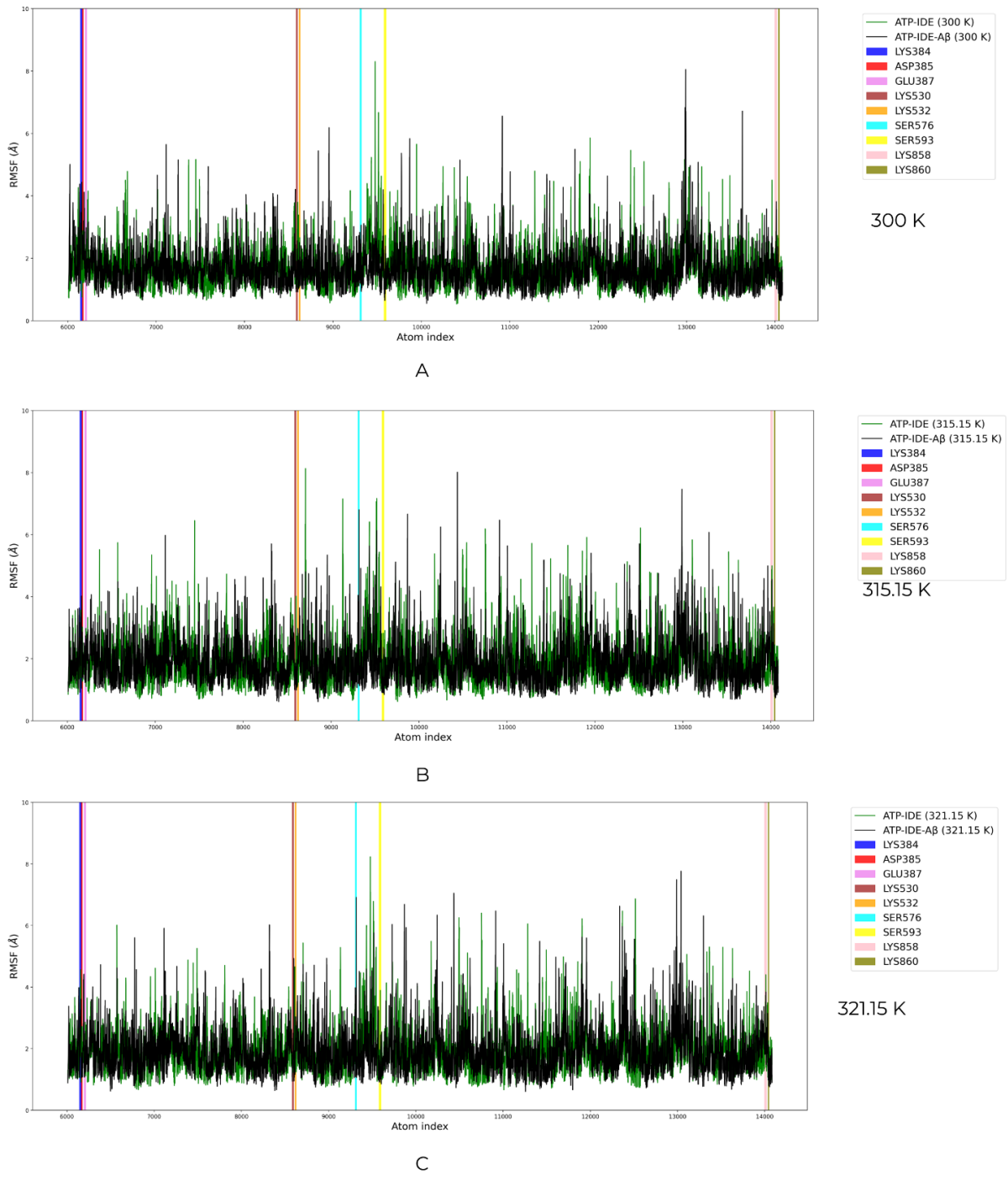

Figure 7. The fluctuations (Å) of backbone atoms in distances between residues LYS384 to LYS860 during the simulations at 300 K (A), 315.15 K (B) and 321.15 K (C). The fluctuations of the backbone atoms in the ATP-IDE system and the ATP-IDE-Aβ system are represented in the green line and the black line, respectively. Vertical bars show the regions of the residues: LYS384 (blue), ASP385 (red), GLU387 (pink), LYS530 (brown), LYS532 (orange), SER576 (cyan), SER593 (yellow), LYS858 (violet) and LYS860 (olive).

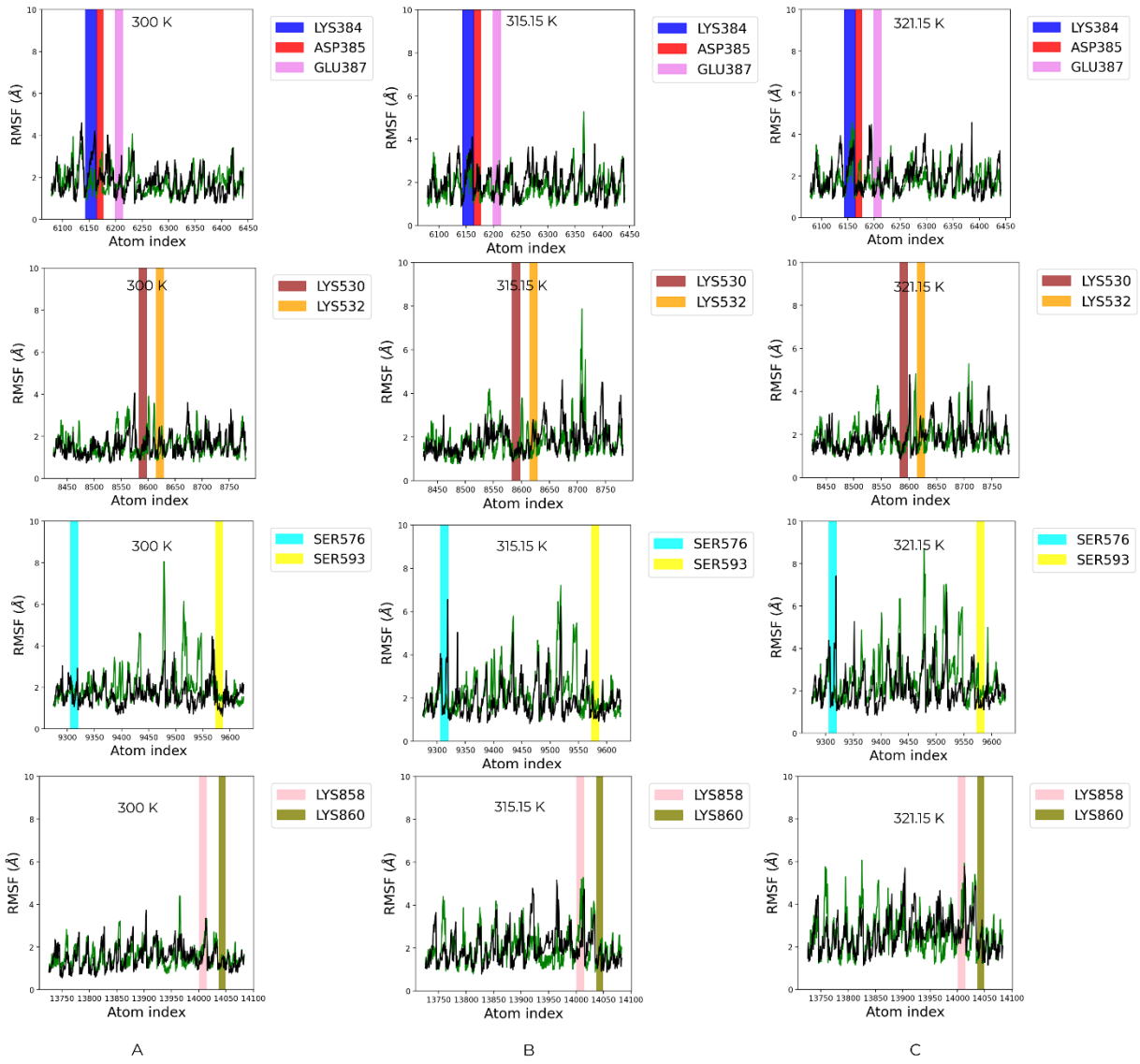

Figure 8. Comparison on the fluctuations (Å) of the backbone atoms of IDE residues at the different temperatures. (A-C) The fluctuations of the backbone atoms at 300 K, 315.15 K and 321.15 K, respectively. Vertical bars show the regions of the residues: LYS384 (blue), ASP385 (red), GLU387 (pink), LYS530 (brown), LYS532 (orange), SER576 (cyan), SER593 (yellow), LYS858 (violet) and LYS860 (olive).

3 CONCLUSIONS

In this study, we employed the molecular docking, the MM equilibration, the QM/MM minimisation and the MD simulation to understand the electrostatic interactions (hydrogen bonds and polar covalent bonds) of the ATP molecule with IDE residues at the ATP-binding domain (allosteric site). We have identified the docked conformers of both the ATP-IDE and the ATP-IDE-Aβ systems using the binding free energy calculation method. We then selected the lowest docked conformers of both the ATP-IDE and the ATP-IDE-Aβ systems as the initial structures for the QM/MM minimisation and the MD simulation. Before the QM/MM minimisation and the MD simulation, we perform the MM equilibration with the conditions of standard atmosphere (pressure (1 atm) and temperature (298 K)).

According to the intermolecular interaction information and the Hirshfeld surface of the hydrogen bonding after QM/MM minimisation, the interaction of the Aβ peptide at the active site of IDE induces the conformational change at the ATP-binding domain, and most of the IDE residues on the surface of the ATP-binding domain serve as the acceptors. Although ATP shifts to neighbouring residues due to the interaction of the Aβ-peptide, a few electrostatic interactions maintain strong interactions: the O3···LYS530(HZ3) interaction and the O3···ASP385(HN) interaction. The Dnorm map illustrates the electron density of the IDE residues at the ATP-binding domain; the ASP385- LYS530 residues have the closest proximity to the ATP. Interestingly, based on topological analysis of electron density (which considers kinetic/potential energies), the hydrogen bonds and polar covalent bonds of ATP with the ASP385- LYS530 residues have stable and strong interactions. Based on the closer proximity of ATP to the ASP385- LYS530 residues and the strong hydrogen bond with the partial covalent bonding interaction between the ATP and ASP385- LYS530 residues, ATP has high binding affinity towards the ASP385- LYS530 residues. The RMSF values of the residues at the surface of ATP-binding domain were calculated after performing the 2000-step MD simulations at the heat-shock temperatures. The results reveal that SER576-LYS858 residues have high flexibilities, whereas ASP385-LYS530 residues have the high thermostabilities.

The results report that the Aβ peptide binding to IDE at the active site can affect the affinity and the stabilities of ATP towards IDE residues at the allosteric site. While many residues at the ATP-binding domain lost the electrostatic interactions resulting from the interaction of the Aβ peptide, the ASP385-LYS530 residues remains stable due to their high affinities. Furthermore, the ASP385-LYS530 residues, and other residues (ASP385, GLU387, LYS530 and LYS532), also have thermostability at the heat-shock temperatures, while SER576-LYS585 residues are the regions of compromised thermostability. In terms of pharmacological drug design, we found that the ASP385-LYS530 residues may be residues of interest for molecular recognition and could be considered for drug targets, and that SER576-LYS585 residues may be mutant forms that influence conformational flexibilities at the heat-shock temperatures. These results provide a deeper understanding of the biological interactions of ATP with the ATP-binding domain within IDE, facilitating the development of allosteric activators/inhibitors of IDE.

AVIALABILITY

github website (somin-s/Supporting_Information_Somin)

SUPPLEMENTARY MATERIALS

The supplementary materials are available in the “supplementary_materials.docx” file.

ACKNOWLEDGEMENTS

The authors thank Rebecca Kambuta for critical reading and advice, and Nina Somin for assistance with figures.

COMPLIANCE WITH ETHICS GUIDELINES

The authors Sarawoot Somin, Don Kulasiria and Sandhya Samarasinghe declare that they have no conflict of interest or financial conflicts to disclose. This article does not contain any studies with human or animal materials performed by any of the authors

REFERENCES

1. Harvey, R., Skelton-Robinson, M., and Rossor, M. (2003) The prevalence and causes of dementia in people under the age of 65 years. Journal of Neurology, Neurosurgery & Psychiatry. 74, 1206-1209
2. Viswanathan, A., and Greenberg, S. M. (2011) Cerebral amyloid angiopathy in the elderly. Annals of neurology. 70, 871-880
3. Pinho, C. M., Teixeira, P. F., and Glaser, E. (2014) Mitochondrial import and degradation of amyloid-β peptide. Biochimica et biophysica acta. 1837, 1069-1074
4. Bates, K. A., Verdile, G., Li, Q. X., Ames, D., Hudson, P., Masters, C. L., and Martins, R. N. (2009) Clearance mechanisms of alzheimer's amyloid-beta peptide: Implications for therapeutic design and diagnostic tests. Molecular psychiatry. 14, 469-486

5. Farris, W., Mansourian, S., Chang, Y., Lindsley, L., Eckman, E. A., Frosch, M. P., Eckman, C. B., Tanzi, R. E., Selkoe, D. J., and Guenette, S. (2003) Insulin-degrading enzyme regulates the levels of insulin, amyloid beta-protein, and the beta-amyloid precursor protein intracellular domain in vivo. Proceedings of the National Academy of Sciences of the United States of America. 100, 4162-4167
6. Shen, Y., Joachimiak, A., Rich Rosner, M., and Tang, W.-J. (2006) Structures of human insulin-degrading enzyme reveal a new substrate recognition mechanism. Nature. 443, 870-874
7. Durham, T. B., Toth, J. L., Klimkowski, V. J., Cao, J. X., Siesky, A. M., Alexander-Chacko, J., Wu, G. Y., Dixon, J. T., McGee, J. E., Wang, Y., *et al.* (2015) Dual exosite-binding inhibitors of insulin-degrading enzyme challenge its role as the primary mediator of insulin clearance in vivo. The Journal of biological chemistry. 290, 20044-20059
8. McCord, L. A., Liang, W. G., Dowdell, E., Kalas, V., Hoey, R. J., Koide, A., Koide, S., and Tang, W.-J. (2013) Conformational states and recognition of amyloidogenic peptides of human insulin-degrading enzyme. Proceedings of the National Academy of Sciences. 110, 13827-13832
9. Noinaj, N., Song, E. S., Bhasin, S., Alper, B. J., Schmidt, W. K., Hersh, L. B., and Rodgers, D. W. (2012) Anion activation site of insulin-degrading enzyme. The Journal of biological chemistry. 287, 48-57
10. Guo, Q., Manolopoulou, M., Bian, Y., Schilling, A. B., and Tang, W.-J. (2010) Molecular basis for the recognition and cleavages of igf-ii, tgf-α, and amylin by human insulin-degrading enzyme. Journal of Molecular Biology. 395, 430-443
11. Perlman, R. K., Gehm, B. D., Kuo, W. L., and Rosner, M. R. (1993) Functional analysis of conserved residues in the active site of insulin-degrading enzyme. The Journal of biological chemistry. 268, 21538-21544
12. Noinaj, N., Bhasin, S. K., Song, E. S., Scoggin, K. E., Juliano, M. A., Juliano, L., Hersh, L. B., and Rodgers, D. W. (2011) Identification of the allosteric regulatory site of insulysin. PLOS ONE. 6, e20864
13. Manolopoulou, M., Guo, Q., Malito, E., Schilling, A. B., and Tang, W. J. (2009) Molecular basis of catalytic chamber-assisted unfolding and cleavage of human insulin by human insulin-degrading enzyme. The Journal of biological chemistry. 284, 14177-14188
14. Song, E. S., Juliano, M. A., Juliano, L., Fried, M. G., Wagner, S. L., and Hersh, L. B. (2004) Atp effects on insulin-degrading enzyme are mediated primarily through its triphosphate moiety. The Journal of biological chemistry. 279, 54216-54220
15. Camberos, M. C., Pérez, A. A., Udrisar, D. P., Wanderley, M. I., and Cresto, J. C. (2001) Atp inhibits insulin-degrading enzyme activity. Experimental biology and medicine (Maywood, NJ). 226, 334-341
16. Del Carmen Camberos, M., and Cresto, J. C. (2007) Insulin-degrading enzyme hydrolyzes atp. Experimental biology and medicine (Maywood, NJ). 232, 281-292
17. Ivancic, V. A., Krasinski, C. A., Zheng, Q., Meservier, R. J., Spratt, D. E., and Lazo, N. D. (2018) Enzyme kinetics from circular dichroism of insulin reveals mechanistic insights into the regulation of insulin-degrading enzyme. Bioscience reports. 38,
18. da Cruz, C. H. B., and Seabra, G. (2014) Molecular dynamics simulations reveal a novel mechanism for atp inhibition of insulin degrading enzyme. Journal of Chemical Information and Modeling. 54, 1380-1390
19. Cornish-Bowden, A. (2014) Understanding allosteric and cooperative interactions in enzymes. The FEBS journal. 281, 621-632
20. Monod, J., Wyman, J., and Changeux, J.-P. (1965) On the nature of allosteric transitions: A plausible model. Journal of Molecular Biology. 12, 88-118
21. Wyman Jr, J., and Allen, D. W. (1951) The problem of the heme interactions in hemoglobin and the basis of the bohr effect. Journal of polymer science. 7, 499-518
22. Kumar, R., Nordberg, A., and Darreh-Shori, T. (2016) Amyloid-β peptides act as allosteric modulators of cholinergic signalling through formation of soluble baβacs. Brain : a journal of neurology. 139, 174-192
23. Naray-Szabo, G., and Ferenczy, G. G. (1995) Molecular electrostatics. Chemical Reviews. 95, 829-847
24. Mladenovic, M., Arnone, M., Fink, R. F., and Engels, B. (2009) Environmental effects on charge densities of biologically active molecules: Do molecule crystal environments indeed approximate protein surroundings? The Journal of Physical Chemistry B. 113, 5072-5082
25. Anderson, A. C. (2003) The process of structure-based drug design. Chemistry & biology. 10, 787-797
26. Hu, Y. C., Zhang, X. H., Li, Q. S., Zhang, Y. H., and Li, Z. S. (2017) Effect of water on the structure and stability of hydrogen‐bonded oxalic acid dimer. Chemphyschem. 18, 3375-3383
27. Kalaiarasi, C., Manjula, S., and Kumaradhas, P. (2019) Combined quantum mechanics/molecular mechanics (qm/mm) methods to understand the charge density distribution of estrogens in the active site of estrogen receptors. RSC Adv. 9, 4758-4771

28. Chen, D., Oezguen, N., Urvil, P., Ferguson, C., Dann, S. M., and Savidge, T. C. (2016) Regulation of protein-ligand binding affinity by hydrogen bond pairing. Science advances. 2, e1501240
29. Bönisch, H., Schmidt, C. L., Bianco, P., and Ladenstein, R. (2005) Ultrahigh-resolution study on pyrococcus abyssi rubredoxin. I. 0.69 a x-ray structure of mutant w4l/r5s. Acta crystallographica Section D, Biological crystallography. 61, 990-1004
30. Wang, J., Dauter, M., Alkire, R., Joachimiak, A., and Dauter, Z. (2007) Triclinic lysozyme at 0.65 a resolution. Acta crystallographica Section D, Biological crystallography. 63, 1254-1268
31. Hirano, Y., Takeda, K., and Miki, K. (2016) Charge-density analysis of an iron–sulfur protein at an ultra-high resolution of 0.48 å. Nature. 534, 281-284
32. Spiegel, K., and Magistrato, A. (2006) Modeling anticancer drug-DNA interactions via mixed qm/mm molecular dynamics simulations. Organic & biomolecular chemistry. 4, 2507-2517
33. Mebs, S., Lüth, A., and Luger, P. (2010) A simple procedure for the derivation of electron density based surfaces of drug-receptor complexes from a combination of x-ray data and theoretical calculations. Bioorganic & Medicinal Chemistry. 18, 5965-5974
34. Egieyeh, S., Egieyeh, E., Malan, S., Christofells, A., and Fielding, B. (2021) Computational drug repurposing strategy predicted peptide-based drugs that can potentially inhibit the interaction of sars-cov-2 spike protein with its target (humanace2). PLoS One. 16, e0245258
35. Kumar, S., and Deshpande, P. A. (2021) Structural and thermodynamic analysis of factors governing the stability and thermal folding/unfolding of sazca. PLoS One. 16, e0249866-e0249866
36. Pipe, S. W., and Kaufman, R. J. (1997) Characterization of a genetically engineered inactivation-resistant coagulation factor viiia. Proceedings of the National Academy of Sciences. 94, 11851-11856
37. Du, J., Dong, J., Du, S., Zhang, K., Yu, J., Hu, S., and Yin, H. (2020) Understanding thermostability factors of barley limit dextrinase by molecular dynamics simulations. Frontiers in molecular biosciences. 7, 51
38. Liu, F., Zhao, Y.-L., Wang, X., Hu, H., Peng, H., Wang, W., Wang, J.-F., and Zhang, X. (2015) Elucidation of enzymatic mechanism of phenazine biosynthetic protein phzf using qm/mm and md simulations. PLoS One. 10, e0139081-e0139081
39. Gao, S., Zhu, S., Huang, R., Li, H., Wang, H., and Zheng, G. (2018) Engineering the enantioselectivity and thermostability of a (+)-γ-lactamase from microbacterium hydrocarbonoxydans for kinetic resolution of vince lactam (2-azabicyclo[2.2.1]hept-5-en-3-one). Applied and environmental microbiology. 84,
40. Bekker, G. J., and Kamiya, N. (2023) Thermal stability estimation of single domain antibodies using molecular dynamics simulations. Methods in molecular biology (Clifton, NJ). 2552, 151-163
41. da Cruz, C. H. B., and Seabra, G. M. (2015) Qm/mm simulations of amyloid-β 42 degradation by ide in the presence and absence of atp. Journal of Chemical Information and Modeling. 55, 72-83
42. Tundo, G. R., Sbardella, D., Ciaccio, C., Bianculli, A., Orlandi, A., Desimio, M. G., Arcuri, G., Coletta, M., and Marini, S. (2013) Insulin-degrading enzyme (ide): A novel heat shock-like protein. The Journal of biological chemistry. 288, 2281-2289
43. Chen, C.-H., Patel, R., Bortolami, A., and Sesti, F. (2020) A novel assay for drug screening that utilizes the heat shock response of caenorhabditis elegans nematodes. PLOS ONE. 15, e0240255
44. Wang, R., Lai, L., and Wang, S. (2002) Further development and validation of empirical scoring functions for structure-based binding affinity prediction. Journal of computer-aided molecular design. 16, 11-26
45. Viry, L., Guillot, B., Guillot, R., Lecomte, C., and Jelsch, C. (2001) Refinement of proteins at subatomic resolution with mopro. J Appl Cryst. 34, 214-223
46. Bader, R. F. W. (1998) A bond path: A universal indicator of bonded interactions. The Journal of Physical Chemistry A. 102, 7314-7323
47. Wick, C. R., and Clark, T. (2018) On bond-critical points in qtaim and weak interactions. Journal of molecular modeling. 24, 142-149
48. Cossard, A., Casassa, S., Gatti, C., Desmarais, J. K., and Erba, A. (2021) Topology of the electron density and of its laplacian from periodic lcao calculations on f-electron materials: The case of cesium uranyl chloride. Molecules (Basel, Switzerland). 26, 4227
49. Shaik, S., Danovich, D., Braida, B., Wu, W., and Hiberty, P. C. (2016) New landscape of electron-pair bonding: Covalent, ionic, and charge-shift bonds. The Chemical Bond II: 100 Years Old and Getting Stronger. 169-211
50. Hilal, R., Aziz, S. G., Alyoubi, A. O., and Elroby, S. (2015) Quantum topology of the charge density of chemical bonds. Qtaim analysis of the c-br and o-br bonds. Procedia Computer Science. 51, 1872-1877